Supporting Information

Properties of Site-Specifically Incorporated 3-Aminotyrosine in Proteins to Study Redox-Active Tyrosines: *E. coli* Ribonucleotide Reductase as a Paradigm

Wankyu Lee,[†,○] Müge Kasanmascheff,[§,○,#] Michael Huynh,[∥] Anthony Quartararo,[†] Cyrille Costentin,[∥,▽] Isabel Bejenke,[§] Daniel G. Nocera,[,∥] Marina Bennati,[*,§] Cecilia Tommos,[*,⊥] and JoAnne Stubbe[*,†,‡]*

Index *Page*

1. Expression and purification of α_3NH_2Y.

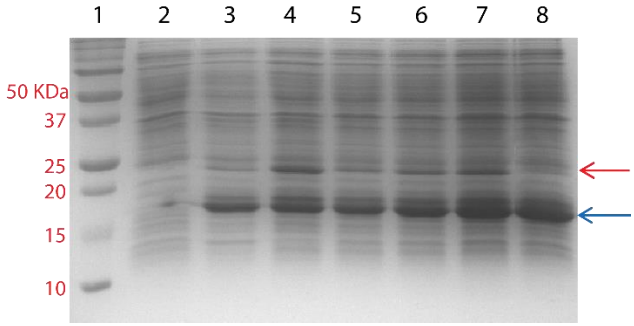

Figure S1. *SDS PAGE analysis of the thioredoxin-α_3NH_2Y expression profile as a function of the NH_2Y-RS induction (OD_{600}).* The gel (15% polyacrylamide) displays in lanes: (1) molecular weight standards, (2) pre-induction sample, (3) post-induction sample from a culture lacking NH_2Y and (4-8) post-induction samples in which NH_2Y-RS was induced by the addition of 0.05% L-arabinose at an OD_{600} of 0.0, 0.4, 0.6, 0.8, and 1.0, respectively. The red and blue arrows indicate the full-length thioredoxin-α_3NH_2Y (21,324 Da) and the truncated thioredoxin-α_3 (17,367 Da) products, respectively.

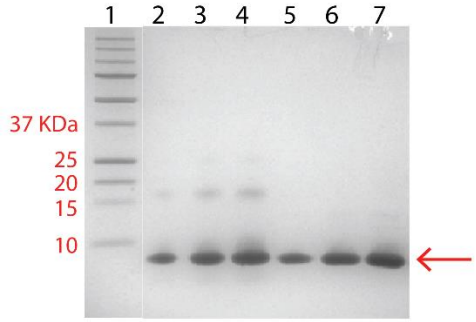

Figure S2. *Tricine SDS PAGE analysis of purified α_3NH_2Y.* Different amounts of isolated of α_3Y (control) and α_3NH_2Y material were analyzed by tricine SDS PAGE to assess purity. The lanes were loaded with: (1) MW standard, (2) 4 μg α_3Y, (3) 8 μg α_3Y, (4) 12 μg α_3Y, (5) 4 μg α_3NH_2Y, (6) 8 μg α_3NH_2Y, and (7) 12 μg α_3NH_2Y. The α_3NH_2Y sample was 99% pure as determined by density quantitation using the QuantityOne software package.

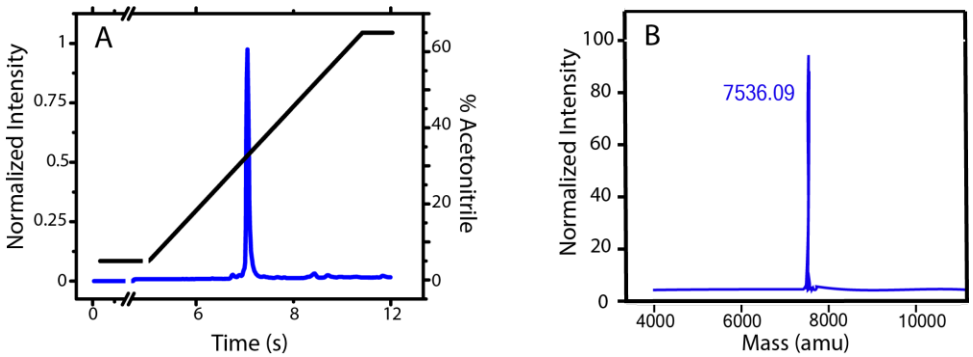

Figure S3. *LC-ESI-MS analysis of purified α_3NH_2Y.* **A.** A typical LC trace shows α_3NH_2Y at 96% purity. Freeze-dried protein was solubilized in water and eluted from a reverse phase column (Agilent Zorbax SB-C3, 2.1 × 150 mm, 5 μm particle size) using a linear gradient with solvent A (water, 0.1% formic acid) and solvent B (acetonitrile, 0.1% formic acid). The flow rate was 0.8 mL/min. The gradient started after five min of 5% B and solvent B was linearly increased from 5 to 65% B over 6

min. The single peak elutes with a retention time of 7.1 min. **B.** A typical de-convoluted ESI-MS trace displays one dominant peak (7536.1 Da) consistent with the prediced average molecular mass of reduced α_3NH_2Y (7535.8 Da).

2. Spectroscopic measurements on α_3NH_2Y. Absorption, circular dichroism (CD) and fluorescence spectra were collected on an Evolution 300 UV-Vis spectrophotometer, an Aviv 202 CD spectrometer, and a Horiba Jobin Yvon Spex Fluorolog spectrofluorometer, respectively. All instruments were equipped with a thermostatted cell holder. An absorption-monitored pH titration (Figure S4A) was conducted by adding (i) 140 µL α_3NH_2Y stock (protein dissolved in 20 mM KPi, 1 mM TCEP, pH 4.7 to an A_{290} of 0.43, 10 mm path length) to 560 µL of 20 mM sodium acetate, 20 mM KPi, 20 mM sodium borate (APB), 1 mM TCEP, pH 4.6 buffer, and (ii) 280 µL α_3NH_2Y stock to 1120 µL of 20 mM APB, 1 mM TCEP, pH 12.6 buffer. The pH titration was performed by equal-volume (~ 0.7 mL) titration mixing the pH 4.7 and 12 protein solutions. UV-Vis settings: path length 10 mm, spectral range 240–500 nm, step size 0.2 nm, scan rate 120 nm min^{-1}, bandwidth 2 nm, and temperature 23 °C.

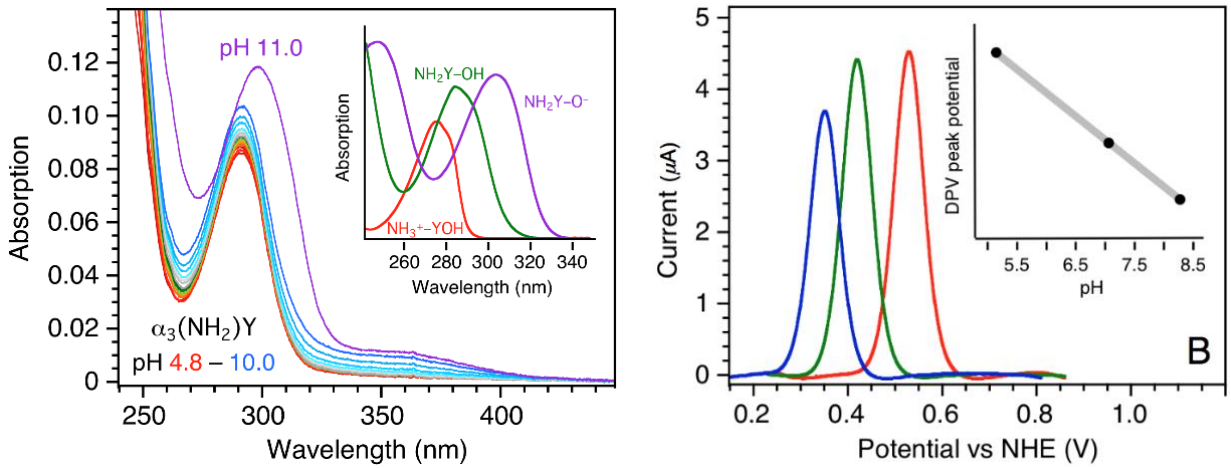

Figure S4. *pH studies of α_3NH_2Y.* **A.** UV-vis spectra of α_3NH_2Y collected between pH 4.8 and 11.0. The pH titration showed that the reduced protein is in the $\alpha_3NH_2Y_{32}$–OH state between pH 4.8 – 10. No blue or red shift was observed in the absorption spectrum. Thus, the phenol NH_2 group remains deprotonated ≥ pH 4.8 and the phenol OH group protonated ≤ pH 10. The insert shows the absorbance spectra of aqueous (aq) NH_2Y, consistent with a previous report[1] and with the pK_a perturbation (1.3 units) observed for α_3Y.[2] **B.** Differential pulse voltammograms of α_3NH_2Y collected at pH 5.1 (red), 7.0 (green) and 8.3 (blue). The peak potential displays a 57 ± 1 mV/pH unit dependence (insert), which is consistent with a $2e^-$, $2H^+$ redox reaction. The pH dependent measurements were conducted with the protein dissolved in the electrolyte solution. Experimental settings: 80 µM α_3NH_2Y in 20 mM APB, 75 mM KCl; equilibration time 5 s, step potential 0.15 mV, modulation time 8 ms, modulation amplitude 50 mV, and temperature 25 °C.

To determine the absolute α-helical content of α_3NH_2Y, its CD spectrum was compared to the CD spectrum of the structurally characterized α_3W protein.[3, 4] Lyophilized α_3NH_2Y and α_3W were dissolved in 20 mM KP_i, 25 µM TCEP, pH 7.2 buffer to a raw 222 nm ellipticity of ~ –170 millidegree (Figure S5A). CD settings: path length 1 mm, spectral range 200–260 nm, step size 0.25 nm, bandwidth 3 nm, time average 3 s, and temperature 25 °C. The protein concentration in the α_3NH_2Y and α_3W CD samples was then determined by using a fluorescence-based method (NanoOrange®; Molecular Probes). A 0–4 µg protein/mL standard curve was prepared by dissolving α_3Y (ε_{277} 1490 M^{-1} cm^{-1}; molecular weight 7520 g mol^{-1}) in 40 mM sodium acetate, pH 5.1. Fluorescence settings: λ_{exc} 485 nm, λ_{em} range 585–600 nm, slit width excitation 2 nm, slit width emission 2 nm, step size 0.5 nm, time average 0.5 s, number of scans 3, and temperature 25 °C. ε_{290} was determined to 3290 ± 140 M^{-1} cm^{-1} for α_3NH_2Y at pH 7.04 ±

0.02. Higher concentrations of the TCEP reducing agent did not give rise to any shift in the protein absorption spectrum and it was concluded that this value represents the fully reduced NH_2-Y_{32} state.

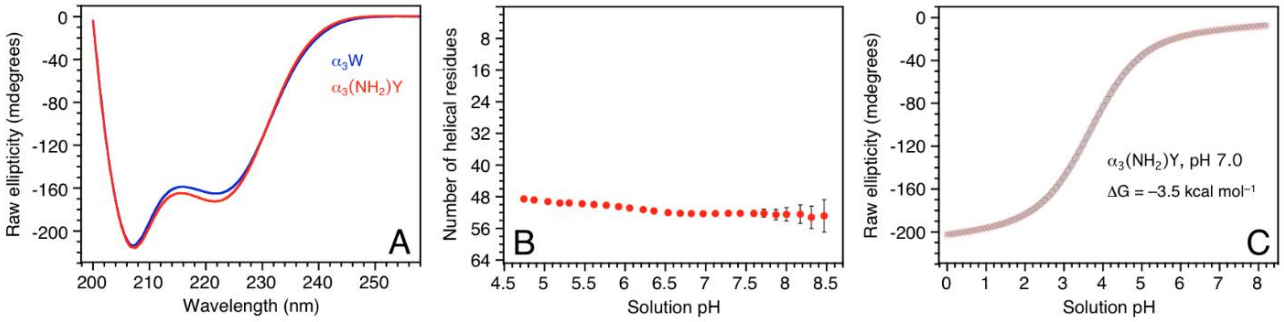

Figure S5. *CD characterization of α_3NH_2Y.* **A.** CD spectra of α_3W (blue) and α_3NH_2Y (red) samples containing 114 ± 3 µM and 112 ± 3 µM protein, respectively. The 222 nm ellipticity (θ_{222}) scales with the α-helical content, which is 78% (51 of 65 residue in total) for α_3W[4] and changes by less than one helical residue between pH 4.5–10.[2] It is 80% (52 of 65) for α_3NH_2Y at pH 7.04 ± 0.02. **B.** Changes in the α-helical content of α_3NH_2Y as a function of pH are minor. The increasing error in the θ_{222} reading > pH 7.7 is due to absorption of TCEP, which precluded data collected above pH 8.5. **C.** The global stability of α_3NH_2Y was determined to –3.5 ± 0.1 kcal mol^{-1} at pH 7.0 by urea denaturation.

CD-based pH titrations (Figure S5B) were conducted by diluting 300 µL protein stock (86 µM α_3NH_2Y, 20 mM KP_i 1 mM TCEP, pH 6.7) into 4.7 mL of 20 mM APB buffer generating two samples with pH 4.7 and pH 11.3, respectively. The pH titrations were performed by automated equal-volume (2.0 mL) titration. CD settings: path length 10 mm, starting pH 4.7, ending pH 10, interval 0.15 pH units, pH dead band 0.05, wavelength 222 nm, bandwidth 3 nm, averaging time 60 s, and temperature 25 °C.

CD-based protein stability measurements (Fig. S5C) were performed by diluting 200 µL protein stock (490 µM α_3NH_2Y, 20 mM KP_i, 540 µM TCEP, pH 7.0) into 2 × 7.5 mL of 20 mM KP_i, 20 mM sodium borate (PB buffer), 3 µM TCEP, pH 7.0, generating two samples containing 0 and 9.37 M urea, respectively. The 9.62 M urea, 20 mM PB, pH 7.0 stock solution was freshly made from ultrapure urea. The denaturation measurements were performed by automated equal-volume (2.0 mL) titration. CD settings: cuvette path length 10 mm, titration steps 0.1 M, equilibrium time 30 s (0–5 M urea) and 60 s (5–8.2 M urea), wavelength 222 nm, bandwidth 3 nm, averaging time 60 s, and temperature 25 °C.

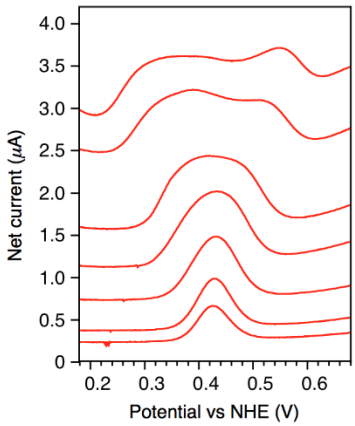

Figure S6. *α_3NH_2Y protein films display "split square-wave voltammogram" response.* The figure shows the SW net current collected at 8 Hz and using a pulse amplitude of (from the bottom) 15, 25, 50, 75, 100, 150 and 175 mV. The net current splits

into two components as the pulse amplitude increases. When combining a low frequency setting (relative to the surface standard electron transfer rate constant, k_{sur}, of the system studied) with a pulse amplitude ramp, this "split SW peaks" response is a characteristic feature observed for redox reactions of strongly adsorbed redox couples.[5, 6] SWV settings: equilibration time, 5 s, step potential 1.05 mV, frequency 8 Hz, pulse amplitude 15–175 mV, and temperature 25 °C.

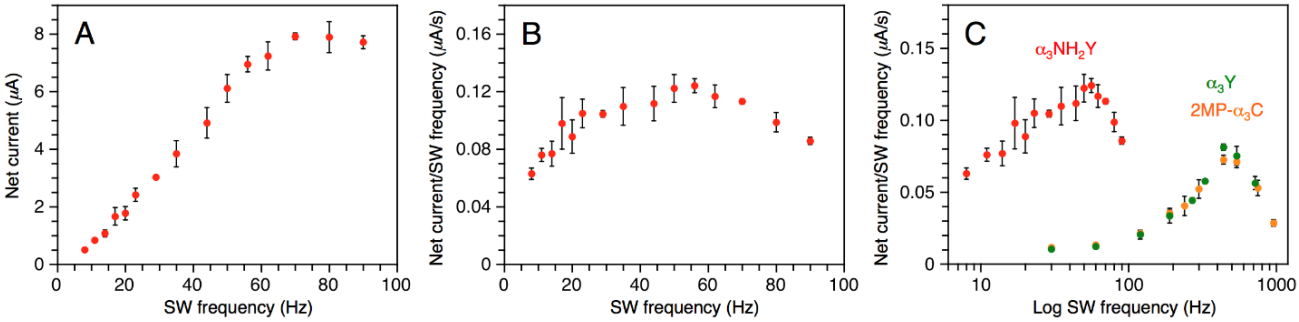

Figure S7. *α_3NH_2Y protein films display a "quasi-reversible maximum" response.* The maximum amplitudes of **A.** the net current and **B** the frequency-normalized net current are displayed as a function of the SW frequency. The parabolic shape of the frequency normalized data in panel **B** is consistent with the "quasi-reversible maximum" (QRM) feature of a surface-confined redox reaction.[5, 7] Panel **C** shows comparable results from α_3Y (green) and 2MP-α_3C (green) (re-analyzed data presented earlier).[8, 9] All three proteins show a QRM, consistent with film formation. The amplitude of the α_3NH_2Y QRM is about two-fold greater than the QRMs of the one-electron α_3Y and 2MP-α_3C redox systems. This is consistent with a two-electron oxidation-reduction process of α_3NH_2Y. SWV settings: equilibration time, 5 s, step potential 1.05 mV, frequency 8–90 Hz SW, pulse amplitude 25 mV, and temperature 25 °C.

3. DFT calculations on 2-aminophenol. DFT calculations were employed to determine the extent to which a trigonal pyramidal perturbation of the NH_2 group in NH_2Y might raise its the reduction potential. Because calculations approximate experimental environments within the bounds of computational feasibility, the following assumptions (and their limitations) were made. To reduce the size of the simulated system, NH_2Y in the full RNR protein structure was modeled as 2-aminophenol (2-NH_2-PheOH) in an implicit water reaction field. The simplified structural model assumes that the protein environment surrounding the tyrosine does not significantly change when the conformation of the NH_2 group changes and treats the protein environment as a constant that is canceled out when comparing relative differences between structural perturbations. The second major assumption in these calculations is that the $1e^- / 1H^+$ pathway is sufficient for estimating the reduction potential of NH_2Y in RNR. While it is possible for an isolated NH_2Y to incur $2e^- / 2H^+$ oxidation, this is unlikely in the biological RNR pathway that manages single electron radical transfers. The final major assumption is that thermodynamic reduction potentials are reflective of experimental reduction potentials in RNR. That is, the actual oxidation of NH_2Y in RNR is subject to kinetic barriers that introduce overpotential on top of the thermodynamic reduction potential. Biological systems may mitigate these kinetic barriers through proton-coupled electron-transfer (PCET). However calculating a reduction potential of a PCET reaction is extremely difficult because it involves sampling pathway-dependent reaction coordinates to determine kinetic barriers of proton and electron transfer. Instead, our DFT calculations follow standard literature procedures[10-12] on fixed thermodynamic states in Scheme S1, thus predicting reduction potentials for the ET/PT and PT/ET pathways, which represent the upper and lower potential limits for the PCET reaction. Notably, the concerted PCET pathway cannot be calculated since the concerted reaction is a kinetic effect that is dependent on the specific path traversed by the electron–proton pair.

Thermodynamic free energies for the PCET square scheme were calculated at each depicted structure for 2-NH_2-PheOH/O• oxidation in Scheme S1 where the NH_2 group is either flat or trigonal

pyramidal. Then, solution-phase reduction potentials[10-12] were computed by using the Born-Haber free energy cycle. Free energies of the products and reactants were determined in the gas phase and then referenced to solvent by calculating the solvation energy for each gas-phase species. The simulations were performed with Gaussian 09, revision D.01 using the B3LYP hybrid DFT functional with Grimme's D3 dispersion correction (Becke-Johnson damping) and the 6-311+G(d,p) basis set.[13, 14] All structures were initially optimized in vacuum with tight geometry. SCF convergence criteria and vibrational frequency analyses verified that optimized structures were local minima, from which enthalpy, entropy, and Gibbs free energies (at T = 298.15 K) were calculated. Solvation free energies for gas-phase optimized structures were computed in water by the SMD polarizable continuum model,[13] which includes corrections for non-electrostatic interactions. For reduction potential calculations, free energies were converted into absolute electrode potentials using the Nernst equation. Importantly, these potentials did not require correction against an experimental reference because we are interested in the difference between these potentials (i.e., the relative potential) as the result of a conformation change—the experimental reference would be treated as a constant value and canceled out when calculating the potential difference. Of the two calculated pathways, since the oxidation occurs at a physiological pH range that is not strong enough to de-protonate the phenol (pKa = 10.1),[1] the ET/PT pathway is more relevant. The "flat" 2-NH_2-PheOH used in this study was free-energy optimized, giving a structure that was not truly flat (0°) but instead had small (<5°) C_4-C_3-N-H_1 and C_2-C_3-N-H_2 angles. When oxidized to 2-NH_2-PheOH +• or 2-NH_2-PheO•, both angles become 0° to obtain a truly flat structure. Conversely, 2-NH_2-PheOH with trigonal pyramidal NH_2 was modeled with the dihedral angle magnitudes constrained to 30° and 50°, matching those previously proposed for NH_2Y_{730}•.[1] Figures S8 and S9 represent the calculation results: a trigonal pyramidal perturbation of the NH_2 group of 2-aminophenol can increase its reduction potential by 190–390 mV. This suggests that a similar increase in the reduction potential of aminotyrosine is still 197–397 mV below the reduction potential of tyrosine in RNR, which means that trigonal pyramidal aminotyrosine can still function as a radial trap and cannot explain why NH_2Y incorporation in RNR still exhibits on-pathway activity.

Scheme S1. PCET Square Scheme of 2-Aminophenol

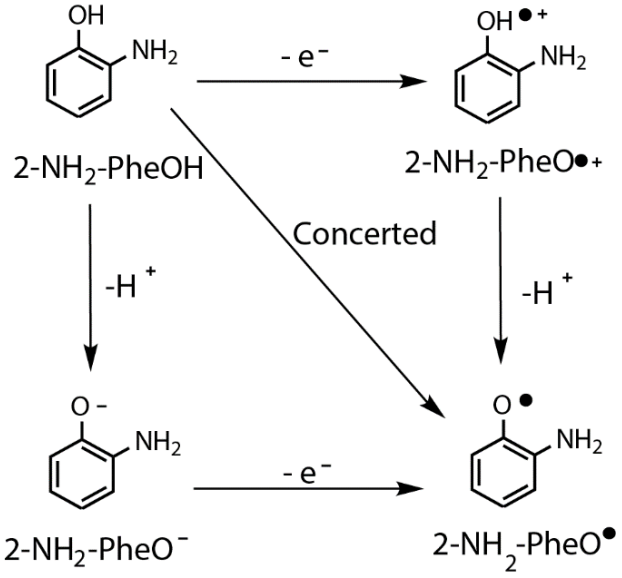

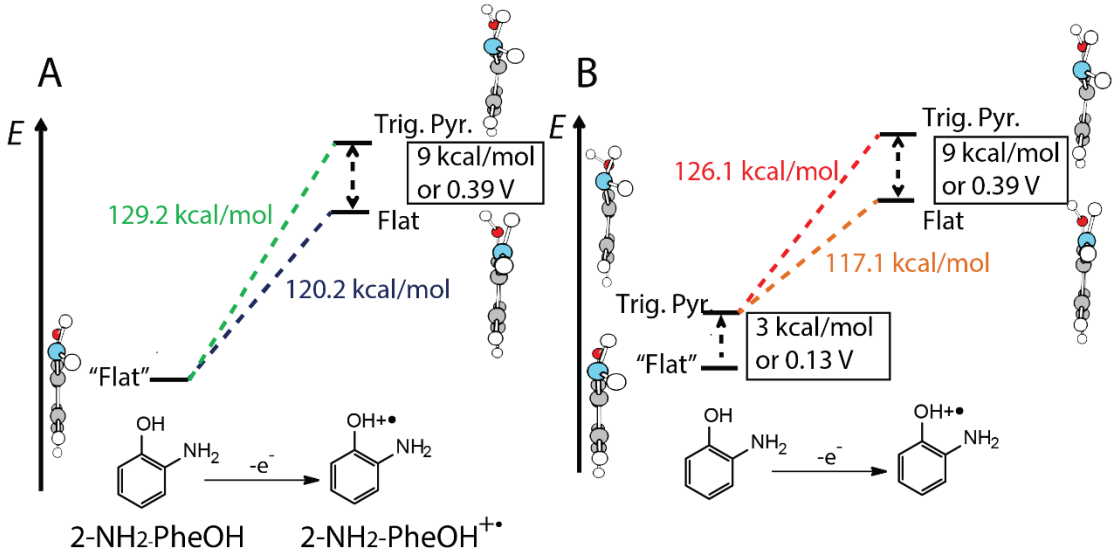

Figure S8. *Effect of NH_2 conformation on 2-NH_2-Phe($OH^{\bullet+}$/OH) couple*. The reduction potentials for oxidation of 2-NH_2-PheOH to 2-NH_2-$PheO^{\bullet+}$ with flat and trigonal pyramidal NH_2 conformations, as determined by DFT calculations, are visualized as energy levels. Note the initial "flat" structure is actually the free energy minimized structure with C-C-N-H dihedral angle magnitudes of 5° and 13°. These angles become zero degrees upon oxidation. Trigonal pyramidal structures are based on a previously implicated structure (C-C-N-H dihedral angles of 30° and 50°).[1] **A.** Starting with flat 2-NH_2-PheOH, oxidation to flat 2-NH_2-$PheOH^{\bullet+}$ requires 120.2 kcal/mol (navy blue) and to trigonal pyramidal 2-NH_2-$PheOH^{\bullet+}$ requires 129.2 kcal/mol (green). **B.** Starting now with trigonal pyramidal 2-NH_2-PheOH, oxidation to flat 2-NH_2-$PheOH^{\bullet+}$ requires 117.1 kcal/mol (orange), while oxidation to trigonal pyramidal 2-NH_2-$PheOH^{\bullet+}$ occurs with 126.1 kcal/mol (red). Thus, oxidation to trigonal pyramidal 2-NH_2-PheOH is harder by 9 kcal/mol, which converts to 0.38 V. Starting with trigonal pyramidal 2-NH_2-PheOH eases the oxidation by 3 kcal/mol or 0.13 V.

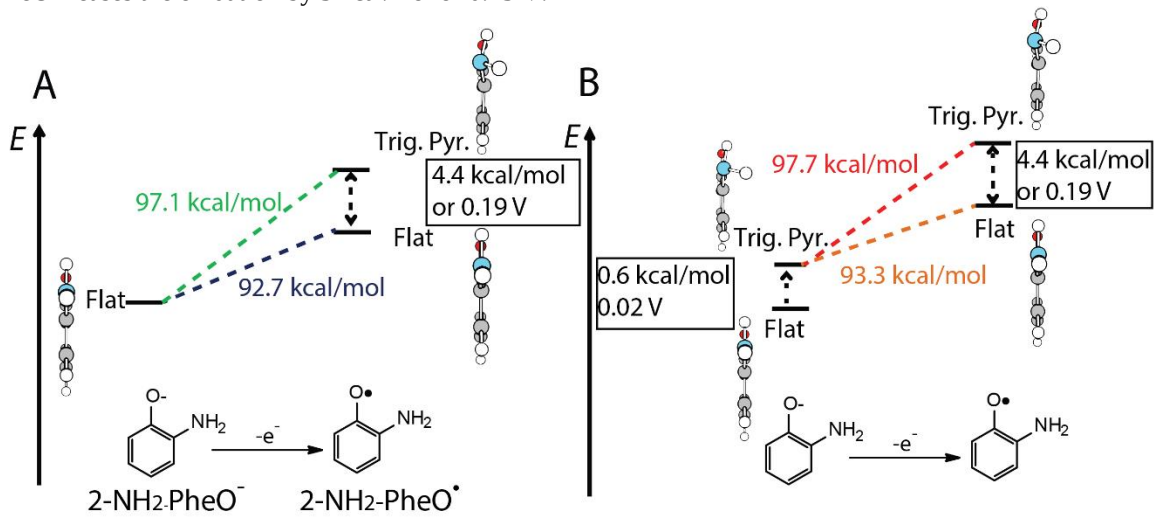

Figure S9. *Effect of NH_2 conformation on the 2-NH_2-Phe($O^{\bullet}$/O^-) redox pair*. The reduction potentials for the oxidation of 2-NH_2-$PheO^-$ to 2-NH_2-$PheO^{\bullet}$ with flat and trigonal pyramidal NH_2 conformations, as determined by DFT calculations, are visualized as energy levels. Trigonal pyramidal structures are based on the EPR structure (C–C–N–H dihedral angle magnitudes of 30° and 50°). **A.** Starting with flat 2-NH_2-$PheO^-$, the oxidation to flat 2-NH_2-$PheO^{\bullet}$ requires 92.7 kcal/mol (navy blue) and to trigonal pyramidal 2-NH_2-$PheO^{\bullet}$ requires 97.1 kcal/mol (green). **B.** Starting with trigonal pyramidal 2-NH_2–$PheO^-$, 2-NH_2-$PheO^-$ oxidizes to flat 2-NH_2-$PheO^{\bullet}$ with 93.3 kcal/mol (orange), while oxidation to trigonal pyramidal 2-NH_2-$PheO^{\bullet}$ occurs with 97.7 kcal/mol (red). Thus, oxidation to trigonal pyramidal 2-NH_2-$PheO^{\bullet}$ is harder by 4.4 kcal/mol

or 0.19 V. Starting with trigonal pyramidal 2-NH_2-$PheO^-$ elevates the potential over flat 2-NH_2-$PheO^-$ by 0.6 kcal/mol or 0.02 V.

4. Synthesis of D_6-NH_2Y. D_6-3-amino-L-tyrosine (D_6-NH_2Y) (1 g) was prepared from D_7-Y (1.3 g) following a previously published protocol[1] and characterized spectroscopically and by mass spectrometry: ^{13}C NMR (600 MHz, D_2O, 25 ºC) δ = 34.7 ppm (quin, C_β, 19.1 Hz), 55.5 ppm (t, C_α, 22.5 Hz), 116.9 ppm (t, arom. C_5, 24.7 Hz), 119.4 (s, arom. C_1), 124.3 ppm (t, arom. C_2, 24.3 Hz), 127.4 (s, arom. C_3), 130.5 ppm (t, arom. C_6, 24.0 Hz), 149.0 ppm (s, arom. C_4), 173.5 ppm (s, COOH). The UV-vis spectrum of D_6-NH_2Y was identical to the spectrum of commercially available NH_2Y. LC-ESI-MS gave a mass of 196.8 Da for D_6-NH_2Y (theoretical mass of 197.1 Da).

9 GHz EPR characterization of reacted His_6-D_6-NH_2Y_{731}-α2/wt-β2/ATP/CDP. The reaction mixture in a final volume of 240 µL contained 20 µM His_6-D_6-NH_2Y_{731}-α2, 20 µM wt-β2 (1.2 Y•/β2)**,** 3 mM ATP, 1 mM CDP. The reaction was initiated by addition of the mutant α2, aged for 25 s at 25 ºC and then quenched in liquid isopentane. EPR spectra were obtained with a Bruker EMX X-band spectrometer at the MIT Department of Chemistry Instrumentation Facility. The instrument was fitted with a quartz finger dewar filled with liquid N_2. WinEPR (Bruker) was used for EPR spin quantitation by comparing the normalized double integral intensity of the reaction spectrum (corrected for number of scans) to the double integral intensity spectrum of a wt-β2 sample with a known Y_{122}• concentration.[15] EPR settings: microwave frequency 9.34 GHz, power 100 µW, modulation amplitude 1.5 G, modulation frequency 100 kHz, time constant 5.12 ms, scan time 41.9 s, and temperature 77 K.

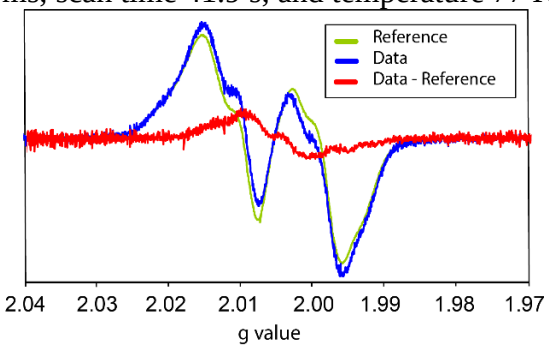

Figure S10. *9 GHz EPR spectra of His_6-D_6-NH_2Y_{731}-α2 reacted with wt-β2, CDP and ATP.* The D_6-NH_2Y_{731}•-α2 spectrum (red), 18% of total spin, was obtained by subtracting the reference Y_{122}•-β2 spectrum (green) from the composite spectrum (blue).

5. Spectral simulations of the multi frequency EPR data. Comparison of 94 GHz EPR spectra of NH_2Y• in D_2O and D_6-NH_2Y• in H_2O clearly reveals the advantages of the deuteration approach (Figure S11).

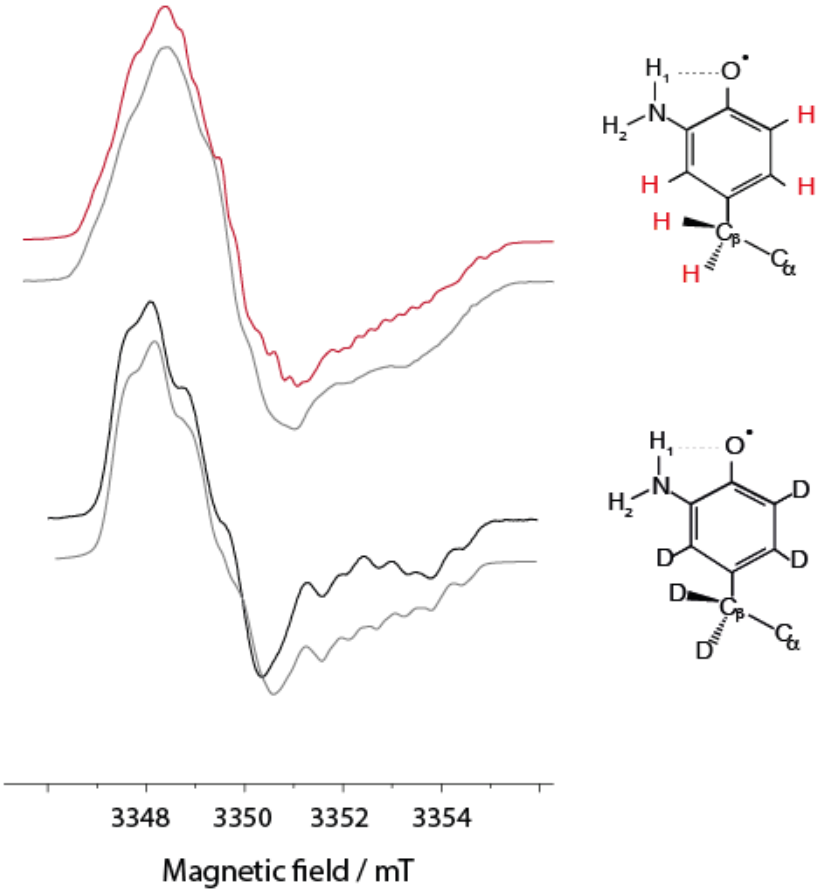

Figure S11. *The EPR spectra of D_6-NH_2Y_{731}• in H_2O (black) recorded at 94 GHz at 80 K compared with H_6-NH_2Y_{731}• in D_2O (red).* Insets display different $^1H/^2H$ labeling for NH_2Y• as well as the numbering for the amino ^1Hs also see Table 1 (main text). The corresponding simulations to a planar structure are shown in grey. Experimental conditions are: π = 40 ns, shot repetition time = 5 ms, shots per point = 80, scans = 108, acquisition time = 12 h.

The EPR spectra of D_6-NH_2Y_{731}• in H_2O recorded at 34, 94 and 263 GHz is compared to simulations for variation of the dihedral angle θ. The RMSD (Root Mean Square Deviation), calculated over all points of the experimental spectrum, is displayed only for 94 GHz. The g values and hfcs are kept constant for the simulations (see main text and Table 1 for details). Only θ is changed between 0 and 50 degrees. Our analysis shows that spectral simulations change significantly when $\theta \geq 20°$.

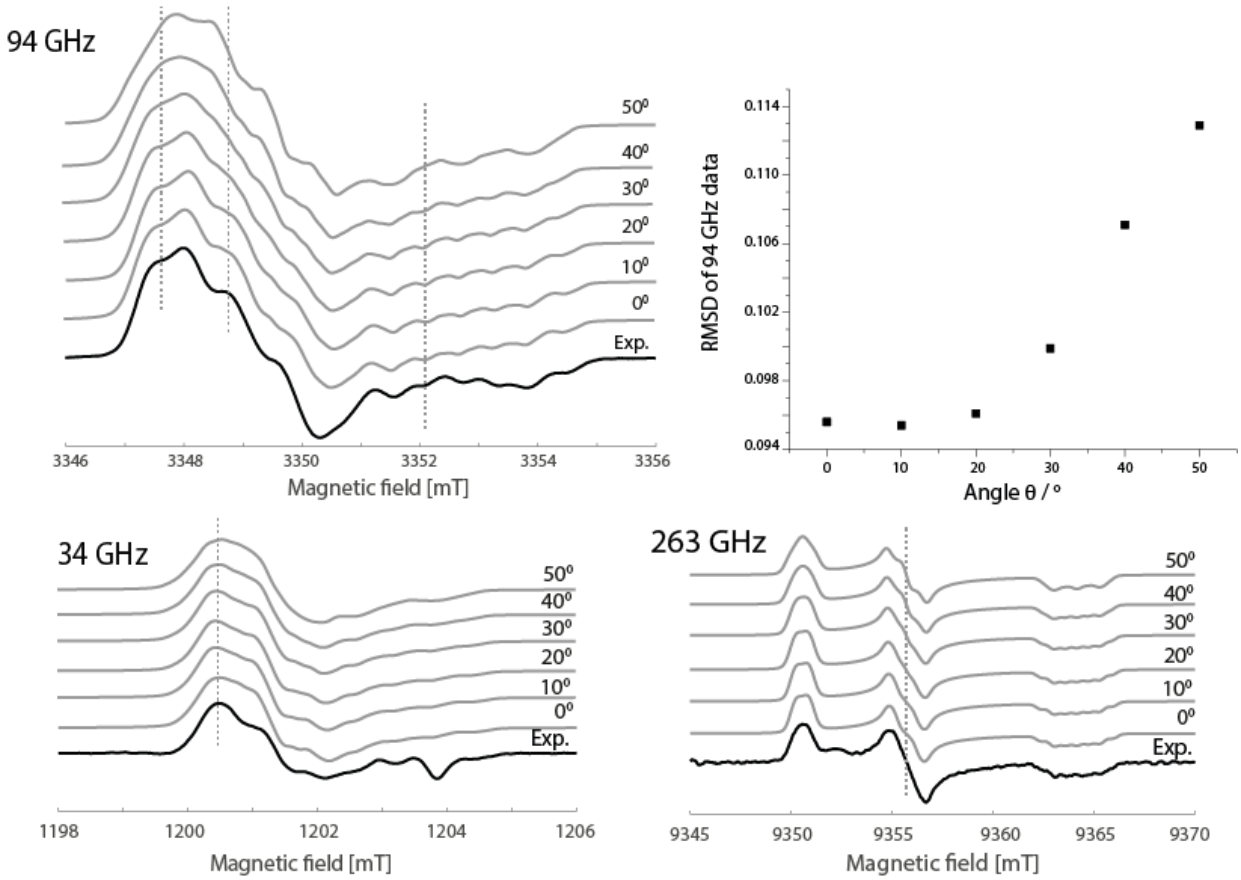

Figure S12. *The EPR spectra of D_6-NH_2Y_{731}• in H_2O buffer (black) recorded at 34 GHz (lower left panel), 94 GHz (upper left panel) and 263 GHz (lower right panel) are shown with corresponding simulations (gray) for variation of the dihedral angle θ.* The *θ* angle used in the simulations are adjacent to the simulated spectra. The upper right panel displays the analysis of the root mean square deviation (RMSD) of the simulation to the 94 GHz data as a function of the angle *θ.*

6. Syntheses of peptides P1 and P2. Sequences for the NH_2Y-containing peptide P1 (amino acids 728-735, H_2N-TL(NH_2Y)YQNTR-COOH) and the Y-containing peptide P2 (H_2N-TLYYQNTR-COOH) from His_6-NH_2Y_{730}-α2 were determined using MS-Digest from Protein Prospector (www.prospector.ucsf.edu). To avoid NH_2Y oxidation, P1 was first synthesized as peptide P3 (H_2N-TL(NO_2Y)YQNTR-COOH) with Fmoc-NO_2Y-OH. Peptide synthesis was carried out using an automated, flow-based peptide synthesizer approach.[16] To couple the first amino acid to the HMPB linker resin, 1 mmol Fmoc-R-OH, 0.5 mmol DIC, and 1 mol percent DMAP were incubated in DMF with ~200 mg of resin for 16 h at room temperature. The resin was washed with ~10 mL DMF followed by ~10 mL DCM before subsequent couplings with the appropriate amino acids in the peptide synthesizer. Automated de-protection of Fmoc was carried out in DMF containing 20% (v/v) piperidine, as described previously.[16] The coupling reactions proceeded as described[16] with 0.4 M protected amino acid, 0.34 M HATU activating agent and 0.7 mmol of DIEA.

P2 and P3 were cleaved from the resin with TFA, as described with no modifications.[16] After cleavage, the crudes were purified by reverse phase HPLC (Agilent Zorbax SB-C18, 21.2 x 250 mm, 5 μm particle size) using a linear gradient with solvent A (water/0.1% TFA) and solvent B (acetonitrile/0.1% TFA). Solvent B was linearly increased from 1 to 61% over 60 min using a flow rate of 4 mL/min. The fractions containing peptide were pooled and lyophilized. The purity was analyzed by LC-ESI-MS. The observed

masses were consistent with the theoretical monoisotopic masses: 1102.5 Da for peptide P3 and 1057.5 Da for peptide P2.

P3 was reduced to peptide P2 with H_2 gas and activated Pd/C catalyst, following a published protocol with no modifications.[1] Briefly, to the stirred solution containing P3 dissolved in 900 μL MeOH and 100 μL H_2O, 5 mg of 10% activated Pd/C catalyst was added. The atmosphere of the reaction mixture was exchanged into $H_{2(g)}$ three times, and the reaction was stirred for 2 h under a $H_{2(g)}$ balloon. After the incubation, the $H_{2(g)}$ was replaced with $N_{2(g)}$ and the catalyst was removed by filtration through a Buchner funnel. We purified peptide P2 by HPLC using the procedure described above. The purity was analyzed by LC-ESI-MS, Figure S13 and the observed mass was consistent with the theoretical monoisotopic mass (1072.5 Da) for P1.

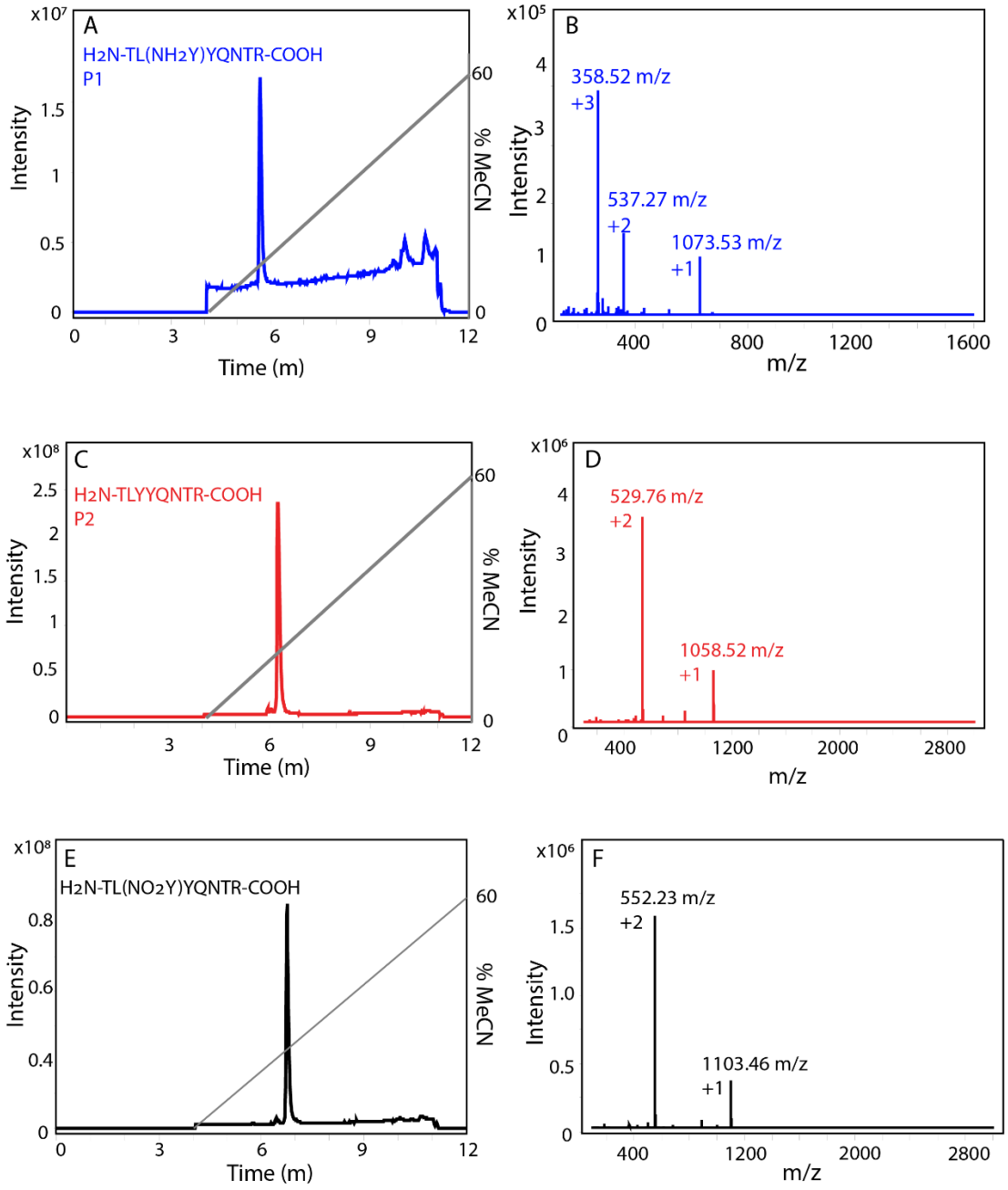

Figure S13. *LC-ESI-MS on purified peptides P1, P2 and P3.* Peptides were eluted from a reverse phase column (Agilent Zorbax SB-C3, 2.1 × 150 mm, 5 µM particle size) using a linear 1 to 61% solvent B over 8 min gradient. **A.** Eluting at 15% B, P1 was 96% pure from LC-MS analysis (blue). The contaminating features above >9 min appear more pronounced for this sample because of the lower ionization efficiency of P1. **B.** The MS shows the +3, +2 and +1 ions consistent with the expected mass of 1073.5 Da. **C.** Eluting at 18% B, P2 was 98% pure from LC-MS analysis (red). **D.** The MS shows the +2 and +1 ions consistent with the expected mass of 1057.5 Da. **E.** Eluting at 22% B, P3 was 97% pure from LC-MS analysis (black). **F.** The MS shows the +2 and +1 ions consistent with the expected mass of 1102.5 Da.

7. MS/MS analysis of the peptides P1 and P2. The trypsin-digested peptide mixture was prepared as described in the main text. The MS/MS experiments were performed with the Agilent 6550 ESI-MS qTOF equipped with a Jupiter C4 reverse phase column (Phenomenex, 1 x 50 mm, 5 µm particle size, 300 Å pore size). The gradient consisted of solvent A (water/0.1% TFA) and solvent B (acetonitrile/0.1%

TFA). Solvent B was linearly increased from 1 to 61% over 34 min with a flow rate of 0.1 mL/min. Prior to the next run, the column was pre-equilibrated with 1% solvent B for 5 min.

The MS procedure for the MS1 was the same as the procedure described in the main text. In the MS/MS, the top 10 most intense ions were selected for fragmentation from the MS scan event and possessed charge states higher than 2+ and lower than 4+. The MS/MS was achieved by CID (collisional induced dissociation) at 26 eV normalized collision energy (NCE) fragmentation with nitrogen employed as the collision gas. The isolation window was set to 2.6 mass units with no offset value. The MS/MS was acquired at 30,000 resolution. A minimum intensity threshold signal of 7E4 was set in order to trigger a MS/MS scan event. The dynamic exclusion time was set to 30 s to avoid repeated sequencing of the same peptides. The MS/MS spectra were obtained by scanning from 100 to 1700 *m/z*.

The MS/MS data were matched to the His_6-NH_2Y_{730}-α2 protein sequence in a database search with the Peaks Studio 8.5 software package (Bioinformatic Solutions Inc.).[17] The precursor mass tolerance error was set to 10 ppm and the product ion mass error was set to 0.2 Da. Up to two missed cleavages were allowed. The variable modifications used in this search were methionine oxidation and 3-aminotyrosine. The resulting protein coverage for His_6-NH_2Y_{730}-α2 was 97%. The high protein coverage lends credence to sufficient trypsin digestion in our non-standard trypsin digestion protocol. The MS/MS corresponding to peptides P1 and P2 are shown in Figure S14. These MS/MS spectra-peptide assignments provided strong evidence for the sequence characterization of the peptides P1 and P2. In addition, the mass of the reduced NH_2Y fragment was verified, important because of possible NH_2Y oxidation.

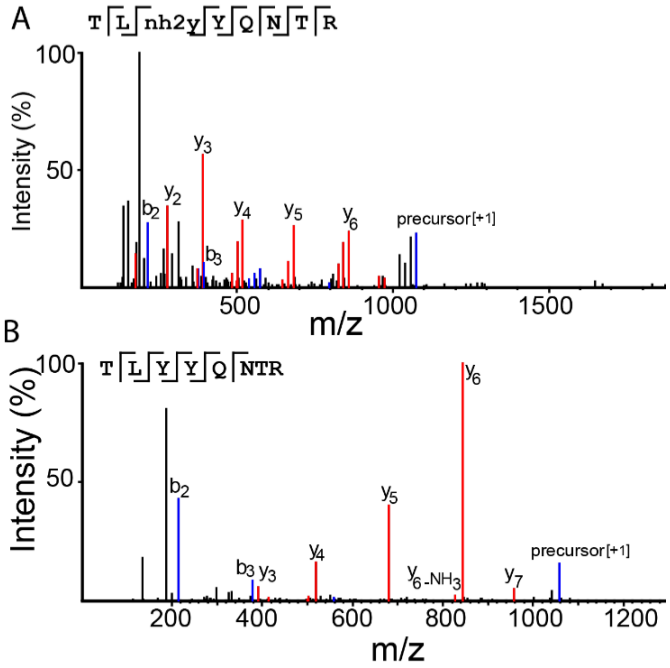

Figure S14. *MS/MS analysis of peptides* (**A**) *P1 and* (**B**) *P2.* The reduced peptide P1 sequence (H_2N-TL(NH_2Y)YQNTR-COOH) was matched to the MS/MS shown in **A**. The peptide P2 sequence (H_2N-TLYYQNTR-COOH) was matched to the MS/MS shown in **B**. For mass spectra, the *b* and *y* fragment ions were denoted in blue and red, respectively.

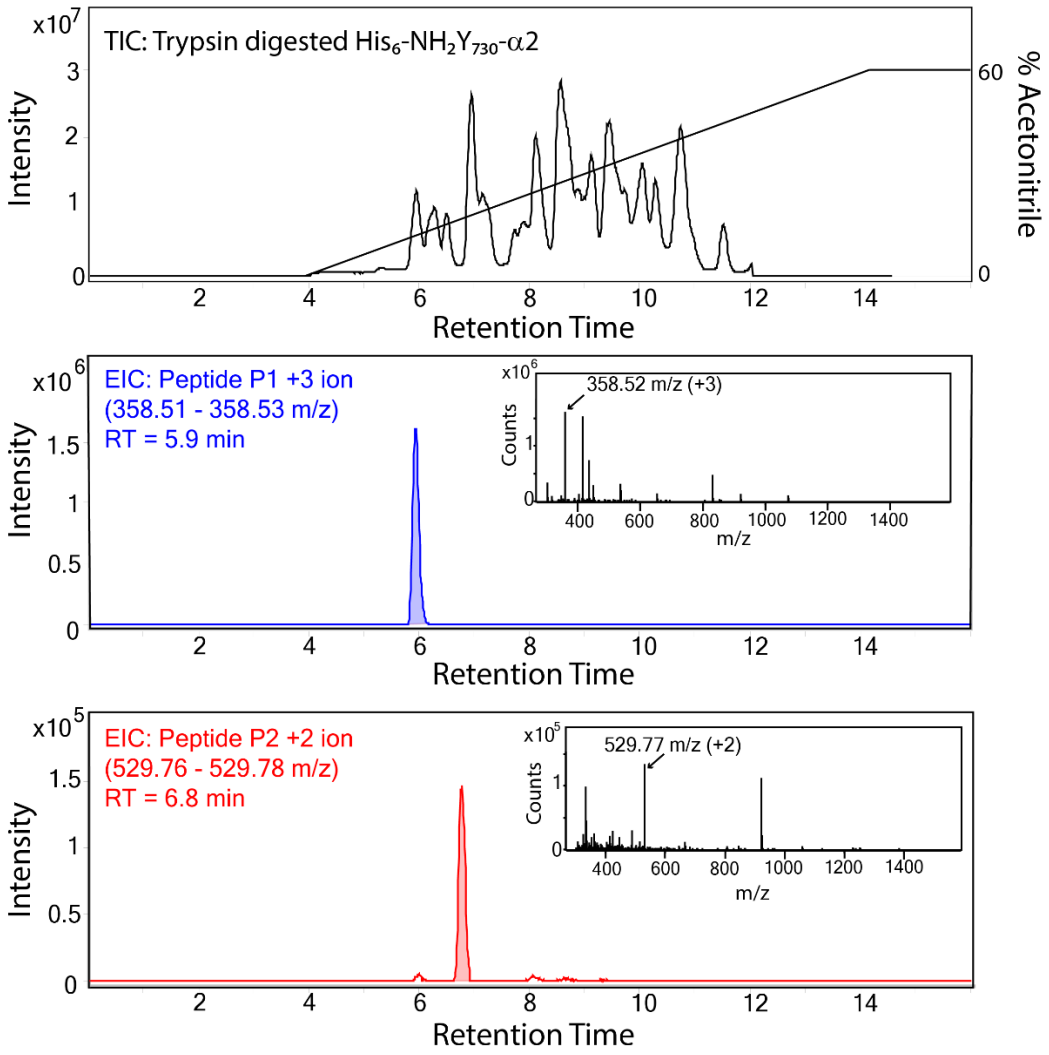

Figure S15. *LC-ESI-MS analysis of the trypsin-digested His_6-NH_2Y_{730}-α2.* Top: Total ion chromatogram (TIC) of the trypsin-digested His_6-NH_2Y_{730}-α2 peptides Middle: The peptide P1 extracted ion chromatogram (EIC) of the +3 ion (358.52 m/z, blue) was generated by isolating a mass window of 358.51 - 358.53 m/z. Peptide P1 elutes at a retention time of 5.9 min. The MS (inset) displays the m/z corresponding to peptide P1. Bottom: The peptide P2 EIC of the +2 ion (529.77 m/z, red) was generated by isolating a mass window of 529.76–529.78 m/z. Peptide P2 elutes at a retention time of 6.8 min. The MS (inset) displays the m/z corresponding to peptide P2.

Table S1. MS quantitation of peptide P1 and P2 by correlation of the peak areas to the standard curves.

Sample	Peptide P1 Amount (ng)	Peptide P2 Amount (ng)	Percent Y contamination
1	2.5 ± 0.1	0.14 ± 0.01	5.6 ± 0.4
2	3.4 ± 0.1	0.21 ± 0.02	6.1 ± 0.5
3	4.0 ± 0.1	0.23 ± 0.01	5.8 ± 0.3
4	4.5 ± 0.1	0.27 ± 0.03	6.0 ± 0.6
5	5.2 ± 0.1	0.31 ± 0.03	6.0 ± 0.6
6	5.9 ± 0.2	0.37 ± 0.03	6.3 ± 0.5
7	6.3 ± 0.2	0.40 ± 0.05	6.3 ± 0.8
8	6.7 ± 0.2	0.45 ± 0.04	6.7 ± 0.6
Average	4.8 ± 0.1	0.30 ± 0.03	**6.1 ± 0.5**

8. Inactivity of NH_2Y-RNRs: issues that play a role in previously observed assays. Given that we measured 6% Y in our LC-MS experiments (main text) and that α is a dimer in rapid equilibrium with monomer, we propose that α2 exists as a mixture of homo and heterodimers of NH_2Y and Y shown in Figure S16 (88%:11.6%:0.4%).

N_3NDP assay: In this assay, the αβ pair containing Y_{122}/Y_{731} in the presence of N_3CDP would produce N•. With the distribution of α2s shown in Figure S16, almost every Y_{731} would result in N•, thus reaching 12%, similar to our previous reports of 14-16%.[18, 19] The main caveat is that in the other α/β pair containing Y_{122}/NH_2Y_{731}, NH_2Y_{731}• might form before Y_{122}/Y_{731} forms N•. If half-site reactivity[20-22] is also prevalent in this construct, the amount of N• would be reduced.

dCDP assay: The 0.7 dCDPs formed in our previous reported one turnover experiments in the absence of external reductant is higher than the predicted 0.21 dCDPs based on our understanding of wt-RNR under the same conditions.[18, 19] The only way to produce more than the expected dCDPs with the αβ pairs containing Y_{122}•/Y_{731} is to have the C-terminal tails of the αβ pairs containing Y_{122}/NH_2Y_{731}• (produced from Y_{122}•/NH_2Y_{731}) re-reduce the disulfides in the active site allowing production of additional dCDPs (Figure S16). This reduction would likely be slow as α2 and β2 need to reorganize into a new complex. The earliest time point in our experiments were obtained at 30 s, while one turnovers can occur on ~100 ms.[23] Thus, it is possible that re-reduction can occur in this timeframe.

To summarize: As noted in the main text, we are unable to quantitatively assess these scenarios but use the preceding arguments to rationalize our earlier results and to now conclude that the NH_2Y-RNRs are inactive.

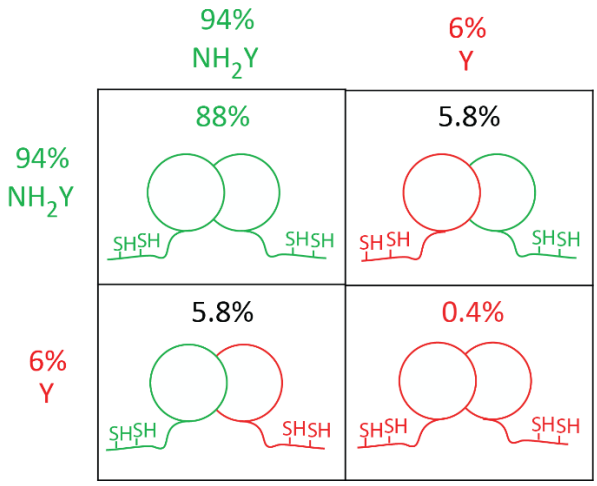

Figure S16. *The statistical distribution of the heterodimeric His_6-NH_2Y_{730}-α/wt-α.* The MS quantitation of the trypsin-digested protein provided evidence for 94% His_6-NH_2Y_{730}-α and 6% His_6-Y_{730}-α. Given these percentages, 88% is His_6-NH_2Y_{730}-α2, 0.4% is His_6-wt-α2 and 12% is His_6-NH_2Y_{730}-α/wt-α of the total α2 population. The thiols located at the *C*-terminal tail of α2 (depicted as SH) allow re-reduction of the active site disulfide produced during dCDP formation. The reduced active site is then ready for an additional turnover.

References

1. Seyedsayamdost, M. R.; Argirevic, T.; Minnihan, E. C.; Stubbe, J.; Bennati, M. (2009) Structural examination of the transient 3-aminotyrosyl radical on the PCET pathway of *E. coli* ribonucleotide reductase by multifrequency EPR spectroscopy. *J. Am. Chem. Soc. 131*, 15729-38.
2. Tommos, C.; Skalicky, J. J.; Pilloud, D. L.; Wand, A. J.; Dutton, P. L. (1999) De novo proteins as models of radical enzymes. *Biochemistry 38*, 9495-507.
3. Ravichandran, K. R.; Zong, A. B.; Taguchi, A. T.; Nocera, D. G.; Stubbe, J.; Tommos, C. (2017) Formal reduction potentials of difluorotyrosine and trifluorotyrosine protein residues: Defining the thermodynamics of multistep radical transfer. *J. Am. Chem. Soc. 139*, 2994-3004.
4. Dai, Q. H.; Tommos, C.; Fuentes, E. J.; Blomberg, M. R. A.; Dutton, P. L.; Wand, A. J. (2002) Structure of a de novo designed model protein of radical systems. *J. Am. Chem. Soc. 124*, 10952-10953.
5. Mirceski, V.; Komorsky-Lovric, S.; Lovric, M. (2007) *Square-wave voltammetry: theory and application*. Springer Science & Business Media.
6. Komorsky-Lovrić, S.; Lovrić, M., Kinetic measurements of a surface confined redox reaction. (1995) *Anal. Chimic. Acta 305*, 248-255.
7. Mirčeski, V.; Lovrić, M., Split square-wave voltammograms of surface redox reactions. (1997) *Electroanalysis 9*, 1283-1287.
8. Berry, B. W.; Martinez-Rivera, M. C.; Tommos, C. (2012) Reversible voltammograms and a Pourbaix diagram for a protein tyrosine radical. *Proc. Natl. Acad.Sci.U. S. A. 109*, 9739-43.
9. Tommos, C.; Valentine, K. G.; Martinez-Rivera, M. C.; Liang, L.; Moorman, V. R. (2013) Reversible phenol oxidation and reduction in the structurally well-defined 2-mercaptophenol-α_3C protein. *Biochemistry 52*, 1409-1418.
10. Cramer, C. J. (2004) Essential of Computational chemistry. *Wiley, England*.
11. Solis, B. H.; Hammes-Schiffer, S. (2011) Theoretical analysis of mechanistic pathways for hydrogen evolution catalyzed by cobaloximes. *Inorg. Chem. 50*, 11252-11262.
12. Baik, M.; Friesner, R. A. (2002) Computing redox potentials in solution: Density functional theory as a tool for rational design of redox agents. *J. Phys. Chem. A 106*, 7407-7412.
13. Marenich, A. V.; Cramer, C. J.; Truhlar, D. G. (2009) Universal solvation model based on solute electron density and on a continuum model of the solvent defined by the bulk dielectric constant and atomic surface tensions. *J. Phys. Chem. B 113* , 6378-6396.
14. Andersson, M. P.; Uvdal, P. (2005) New scale factors for harmonic vibrational frequencies using the B3LYP density functional method with the triple-ζ basis set 6-311+ G (d, p). *J. Phys. Chem. A 109*, 2937-2941.
15. Palmer, G. (1967) Electron paramagnetic resonance. *Methods Enzymol. 10*, 594-610.
16. Mijalis, A. J.; Thomas III, D. A.; Simon, M. D.; Adamo, A.; Beaumont, R.; Jensen, K. F.; Pentelute, B. L. (2017) A fully automated flow-based approach for accelerated peptide synthesis. *Nat. Chem. Biol. 13* (5), 464-466.
17. Fenyö, D. (2000) Identifying the proteome: software tools. *Curr. Opin. Chem. Biol. 11*, 391-395.
18. Minnihan, E. C.; Seyedsayamdost, M. R.; Uhlin, U.; Stubbe, J. (2011) Kinetics of radical intermediate formation and deoxynucleotide production in 3-aminotyrosine-substituted *Escherichia coli* ribonucleotide reductases. *J. Am. Chem. Soc. 133*, 9430-40.
19. Seyedsayamdost, M. R.; Xie, J.; Chan, C. T.; Schultz, P. G.; Stubbe, J. (2007) Site-specific insertion of 3-aminotyrosine into subunit α2 of *E. coli* ribonucleotide reductase: direct evidence for involvement of Y_{730} and Y_{731} in radical propagation. *J. Am. Chem. Soc. 129*, 15060-71.
20. Salowe, S. P.; Ator, M. A.; Stubbe, J. (1987) Products of the inactivation of ribonucleoside diphosphate reductase from *Escherichia coli* with 2'-azido-2'-deoxyuridine 5'-diphosphate. *Biochemistry 26*, 3408-16.
21. Seyedsayamdost, M. R.; Chan, C. T.; Mugnaini, V.; Stubbe, J.; Bennati, M. (2007) PELDOR spectroscopy with DOPA-β2 and NH_2Y-α2s: distance measurements between residues involved in the radical propagation pathway of *E. coli* ribonucleotide reductase. *J. Am. Chem. Soc. 129*, 15748-9.

22. Ravichandran, K. R.; Minnihan, E. C.; Wei, Y.; Nocera, D. G.; Stubbe, J. (2015) Reverse electron transfer completes the catalytic cycle in a 2,3,5-trifluorotyrosine-substituted ribonucleotide reductase. *J. Am. Chem. Soc. 137*, 14387-95.
23. Ge, J.; Yu, G.; Ator, M. A.; Stubbe, J. (2003) Pre-steady-state and steady-state kinetic analysis of *E. coli* class I ribonucleotide reductase. *Biochemistry 42*, 10071-83.